

Quantum Size Effect on Dielectric Properties of Ultrathin Metallic Film: A First-Principles Study of Al(111)

Wenmei Ming,¹ Steve Blair,² and Feng Liu^{1,*}

¹*Department of Materials Science and Engineering, University of Utah, Salt Lake City, UT 84112*

²*Department of Electrical and Computer Engineering, University of Utah, Salt Lake City, UT 84112*

(Dated: March 1, 2022)

Quantum manifestations of various properties of metallic thin films by quantum size effect (QSE) have been studied intensively. Here, using first-principles calculations, we show quantum manifestation in dielectric properties of Al(111) ultrathin films. The QSE on the dielectric function is revealed, which arises from size dependent contributions from both intraband and interband electronic transitions. More importantly, the in-plane interband transitions in the films thinner than 15 monolayers are found to be smaller than the bulk counterpart in the energy range from 1.5 eV to 2.5 eV. This indicates less energy loss with plasmonic material of Al in the form of ultrathin film. Our findings may shed light on searching for low-loss plasmonic materials via quantum size effect.

PACS numbers: 78.20.Ci, 68.55.jd, 71.15.Mb, 73.61.At

I. INTRODUCTION

When the dimension of a material (either one, two or all three dimensions) is reduced to nanoscale, its properties become size dependent, due to quantum confinement effect or surface effect, and the former is generally referred to as the quantum size effect (QSE)^{1,2}. In recent years, there have been intensive studies of QSE on properties of ultrathin films in the quantum confinement regime. In particular, when the thickness of a metal film is comparable with the electron Fermi wavelength, quantum confinement becomes prominent resulting in discretization of electronic states (quantum-well states). This in turn leads to a variety of strongly thickness-dependent film properties, manifested as QSE, such as surface energy^{3,4}, surface stress^{5,6}, surface diffusion barrier^{7,8}, surface reactivity⁹, work function¹⁰, elastic constant¹¹ and so on.

Furthermore, considering the emerging field of plasmonics^{12–14} for myriad applications, the QSE is expected to also affect the dielectric and optical properties of ultrathin metal films. Theoretically, Dryzek *et al*¹⁵ and Apell *et al*¹⁶ showed QSE on the optical spectra of gold and potassium thin films, respectively, within finite free electron model, which differs from the classical Drude model. Laref *et al*¹⁷ studied the thickness dependence of optical permittivity of ultrathin gold films for a more accurate design of plasmonic device, based on density functional theory (DFT) calculations. Experimentally, Kuzik *et al*^{18,19} observed the periodic oscillation of optical conductivity as a function of film thickness in Nb, Cu, Mo, W, Ni and Ti, which is possibly an indication of QSE.

Generally, the simple metals (e.g. Ag, Au, Cu, Al and Mg) are good candidates to generate plasma, because they have a high free carrier density around Fermi level that leads to a large bulk plasma frequency of about 10 eV. This makes the workable frequency of the exter-

nally applied electromagnetic field cover a wide range from visible to ultraviolet (UV). However, one problem with using these metals is the large energy loss of the applied electromagnetic field, largely because the absorption induced by interband electronic transitions falls also into the visible and UV range^{12,20}. Band structure engineering, therefore, is required to remove the interband transitions or push them out of visible and UV range, especially for UV plasmonic applications. One interesting idea is to reduce the thickness of metal films so that one may take the advantage of QSE to reduce the absorption in the frequency range of interest. This idea has motivated the present study of QSE on the dielectric properties of ultrathin Al(111) films.

We have investigated the QSE on the dielectric function of Al(111) films with both intraband and interband contributions in the thickness range from 1 monolayer (ML) to 39 MLs, using first-principles DFT calculations within the random phase approximation (RPA)²¹. We found that the plasma frequency is reduced due to the transfer of electronic transition strength from the intraband to interband transitions and the amount of such reduction oscillates as a function of film thickness. Also, we found that for the films thinner than 15 MLs, the imaginary part of in-plane dielectric constant with energy greater than 1.5 eV is decreased to be smaller than the bulk value. This may translate into less energy loss in the plasmonic devices made of Al(111) films thinner than 15 MLs.

II. CALCULATION DETAILS AND THEORY

Our DFT calculations were performed by using projector augment wave pseudopotential (PAW)²² with the generalized gradient approximation (GGA)²³ to the exchange-correlation functional, as implemented in VASP package²⁴. The Al(111) slab plus a more than 20

Å vacuum was used as our model film structure. 350 eV energy cutoff and $61 \times 61 \times 1$ Γ -centered k-mesh were used for wavefunction expansion and k-space integration, respectively, to achieve a highly converged dielectric function calculation. All the structures were relaxed in terms of internal atomic coordinates using conjugate gradient method until the force exerted on each atom is smaller than $0.01 \text{ eV}/\text{\AA}^3$. For a better bulk reference, we used a hexagonal unit cell with three Al(111) layers without vacuum, and the same energy cutoff and in-plane k-point sampling as the slab calculation to calculate the bulk Al dielectric function. The in-plane lattice constant of 2.8567 \AA for Al(111) film was used.

In general, the optical absorption results from three mechanisms: plasmon resonance, free carrier intra-band damping and bound electron inter-band transitions. The first one is responsible for exciting plasma in plasmonic devices, but the latter two are detrimental to the performance of plasmonic devices. In this work, we focus on possible reduction of absorption due to the latter two mechanisms by QSE, so the absorption from plasmon resonance is not considered. For the absorption from plasmon resonance in nanostructures, the nonlocal part of the dielectric function may have a noticeable effect on the adsorption spectra because of the plasmon-resonance induced large non-uniform electric field distribution that cannot be described by local electrodynamics. However, for free carrier intra-band damping and bound electron inter-band transitions, connecting the optical adsorption to the local description of dielectric function is generally valid as long as the optical wavelength is much larger than the unit-cell dimension and the thickness of the film. This approximation has been successfully used in calculating the optical properties of low dimensional structures, such as nanotubes²⁵, graphene systems²⁶ and nanowires²⁷. Therefore, we also used the local dielectric function to investigate the optical absorption from electron intra-band damping and inter-band transitions.

In a partially filled metal like Al, the intraband transitions around Fermi energy need also to be included, in addition to the interband transitions. The interband-transition contribution to the dielectric function is in the form of 2nd rank tensor and its imaginary part is expressed as²⁸:

$$\varepsilon_{\alpha\beta}^{2,inter}(\omega) = \frac{8\pi^2 e^2}{\Omega m^2 \omega^2} \sum_{n \neq m; k} (f_{mk} - f_{nk}) P_{e_\alpha; m, n, k} P_{e_\beta; m, n, k} \times \delta(\epsilon_{mk} - \epsilon_{nk} - \hbar\omega) \quad (1)$$

Where Ω is the volume of the unit cell, f_{nk} is Fermi-Dirac occupation function. e_α is the unit Cartesian directional vector of electric field polarization and ϵ_{nk} is the electron eigen-energy. $P_{e_\alpha; m, n, k}$ is the momentum matrix element between the Bloch wavefunctions of (m, k) and (n, k) with the projection onto the e_α direction. The corresponding real part can be computed by Kramers-Kronig relation.

The intraband-transition contribution to the dielectric

function is usually expressed in Drude form:

$$\varepsilon_{\alpha\beta}^{2,intra} = \pi \omega_{pl; \alpha\beta}^2 \frac{\partial \delta(\omega)}{\partial \omega} \quad (2)$$

$\omega_{pl; \alpha\beta}^2$ is a tensor which coincides with the bulk plasma frequency tensor in bulk calculation and follows the expression:

$$\omega_{pl; \alpha\beta}^2(\omega) = \frac{8\pi^2 e^2}{\Omega \hbar^2 m^2} \sum_{n, k} 2\delta(\epsilon_{nk} - \epsilon_F) (e_\alpha \frac{\partial \epsilon_{nk}}{\partial k}) (e_\beta \frac{\partial \epsilon_{nk}}{\partial k}) \quad (3)$$

This equation gives the imaginary part of intraband dielectric function within the independent particle picture, where the electron lifetime is infinite. However, the scattering from electron-electron, electron-phonon and electron-defect interactions may result in a finite lifetime. Thus, a lifetime broadening parameter Γ is often introduced in order to compare the experimental dielectric function with the calculated one. The equation is then modified to include this free carrier intra-band damping:

$$\varepsilon_{\alpha\beta}^{2,intra}(\omega) = \frac{\Gamma \omega_{pl; \alpha\beta}^2}{\omega(\omega^2 + \Gamma^2)}. \quad (4)$$

The film volume excluding the vacuum region from the supercell was used to normalize the dielectric function in the above equations. The interband transitions and intraband damping induced optical absorption energy loss per unit volume is proportional to the imaginary part of the dielectric function^{29,30}.

The interband and intraband dielectric functions are coupled with each other through the f -sum rule as³¹:

$$\int_0^\infty \omega [\varepsilon_{\alpha\alpha}^{2,intra}(\omega) + \varepsilon_{\alpha\alpha}^{2,inter}(\omega)] d\omega = \frac{2\pi^2 e^2 n \hbar^2}{m} \quad (5)$$

Where n is the valence electron number density. In the following section this sum-rule will be used to explain the difference between slab plasma frequency and bulk plasma frequency.

III. RESULTS AND DISCUSSION

Bulk Al has a high plasma frequency of about 12.4 eV and its dielectric properties as a function of incident photo energy were studied by previous studies³². The most striking feature from the imaginary part of dielectric function is that it has two interband absorption peaks around 0.5 eV and 1.5 eV due to the transitions between parallel bands with energy difference of 0.5 eV and 1.5 eV, respectively. For the thin film form of Al(111), because the interlayer distance and the half electron Fermi wavelength have a simple ratio of about 4:3, it suggests a strong QSE³³, similar to the case of Pb(111) thin film with a ratio close to 3:2³. We expect the quantum manifestation in the plasma frequency and interband transitions will appear in Al(111) ultrathin films. To illustrate

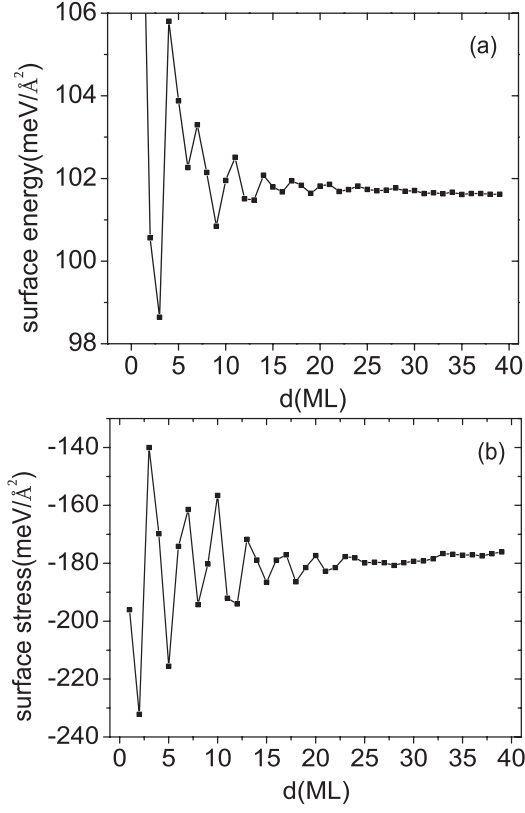


FIG. 1: (a) Surface energy of free-standing Al(111) film as a function of thickness in unit of monolayer; (b) The corresponding surface stress.

the possible QSE, we first calculated surface energy and surface stress as a function of film thickness, as shown in Fig. 1. Clearly, surface energy in Fig. 1(a) displays an oscillation with a 3 ML periodicity superimposed by a 10 ML beating pattern, especially for the first 30 MLs, in good agreement with previous result³⁴. The 3 ML periodicity corresponds to the film thickness at which the electron forms a standing-wave and the 10 ML beating pattern arises from the imperfect matching between interlayer distance and half Fermi wavelength. Surface stress displays also a QSE-induced oscillation, as showed in Fig. 1(b).

Next, we calculated the in-plane plasma frequency as a function of film thickness in Fig. 2(a), which shows the film thickness dependence of intraband contribution to the dielectric function as defined in equation (4). First, there is a very fast decay of plasma frequency from 14.3 eV to 10.5 eV going from the 1 ML to 3 ML film. Second, there appears also a 3 ML oscillation pattern in the plasma frequency. To understand these observations, we noticed from equation 3 that the squared plasma frequency will be proportional to the electron density of states (DOS) at the Fermi energy if $e_\alpha \frac{\partial \epsilon_{nk}}{\partial k}$ varies very slowly with k or remains constant. Therefore, we calculated the DOS at the Fermi energy at different film thickness in Fig. 2(b). It shows a very similar oscillation

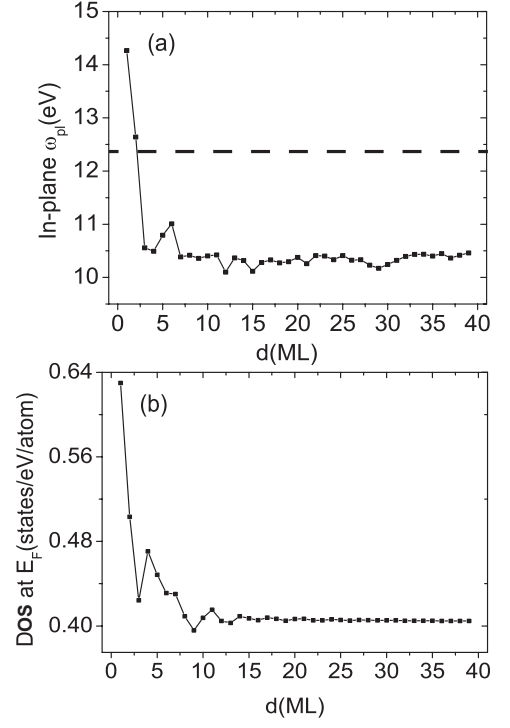


FIG. 2: (a) The slab plasma frequency (in eV) as a function of Al(111) film thickness. The dashed line indicates the bulk plasma frequency. (b) the electron density of states (DOS) at Fermi energy as a function of film thickness.

tion pattern as the plasma frequency in Fig. 2(a). In particular, the DOS drops significantly from the 1 ML, 2 ML to 3 ML film and then converges quickly to the bulk value with further increasing film thickness. We thus attributed the large plasma frequency of the ultra-thin 1 ML, 2 ML and 3 ML films to their large DOS at the Fermi energy. However the oscillation pattern of plasma frequency does not match exactly in a one-to-one fashion to that of DOS at the Fermi energy. This may be related to the modulation of $e_\alpha \frac{\partial \epsilon_{nk}}{\partial k}$ term in equation (3) by QSE, which is also thickness dependent.

We also calculated the in-plane plasma frequency of bulk Al with both 3 ML and 39 ML unit cells and obtained the same value of 12.4 eV. However, from Fig. 2(a) the slab plasma frequency shows sizable deviation from its bulk value even for the film thickness of 39 MLs. The similar difference has been previously reported for Cu(110)²¹ and for Au(111)¹⁷ surfaces. It depends on the metal species and surface orientation. Physically the calculated in-plane plasma frequency in the slab setup should converge to its bulk value in the limit of infinite film thickness. This in turn means the thickness used in our calculation is still not thick enough to reach the bulk value. Such a difference can be qualitatively understood from the finite free-electron gas model^{35–38}: with finite film thickness, the contribution of interband transitions due to quantum confinement induced energy level discreteness to the dielectric function inversely depends on

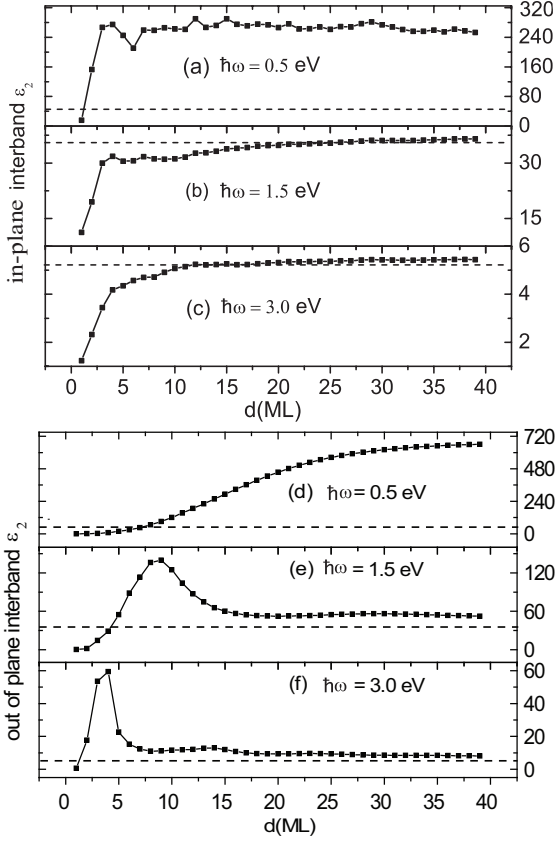


FIG. 3: The imaginary part of interband in-plane dielectric function at three different energies: (a) $\hbar\omega = 0.5$ eV; (b) $\hbar\omega = 1.5$ eV; (c) $\hbar\omega = 3.0$ eV. The imaginary part of interband out-of-plane dielectric function at three different energies: (d) $\hbar\omega = 0.5$ eV; (e) $\hbar\omega = 1.5$ eV; (f) $\hbar\omega = 3.0$ eV. The dashed lines indicate the corresponding bulk values.

the film thickness, which will vanish in the bulk limit and leave only the commonly termed intraband contribution to the dielectric function. With the f -sum rule considered then the intraband contribution will proportionally increase towards the bulk, so that the slab plasma frequency will be smaller than the bulk value and converge to bulk plasma frequency with increasing thickness. On the other hand, we noticed that in terms of dielectric function bulk Al cannot be fully described by free electron model, because it has finite interband contribution for all frequencies from high to even $\omega \rightarrow 0$ eV^{39,40}, hence Al is expected to have more complex dielectric function profile as a function of thickness than that predicted from finite free electron gas model as we will see from the results below.

Next, we investigated QSE on the interband contribution to the dielectric function. In Fig. 3 we plotted the imaginary part of the in-plane ϵ_2 versus film thickness for three different photon energies ($\hbar\omega = 0.5$ eV, 1.5 eV and 3.0 eV). The dashed line in each plot represents the corresponding bulk value at the same energy. We can see that the value at $\hbar\omega = 0.5$ eV is much larger than that in

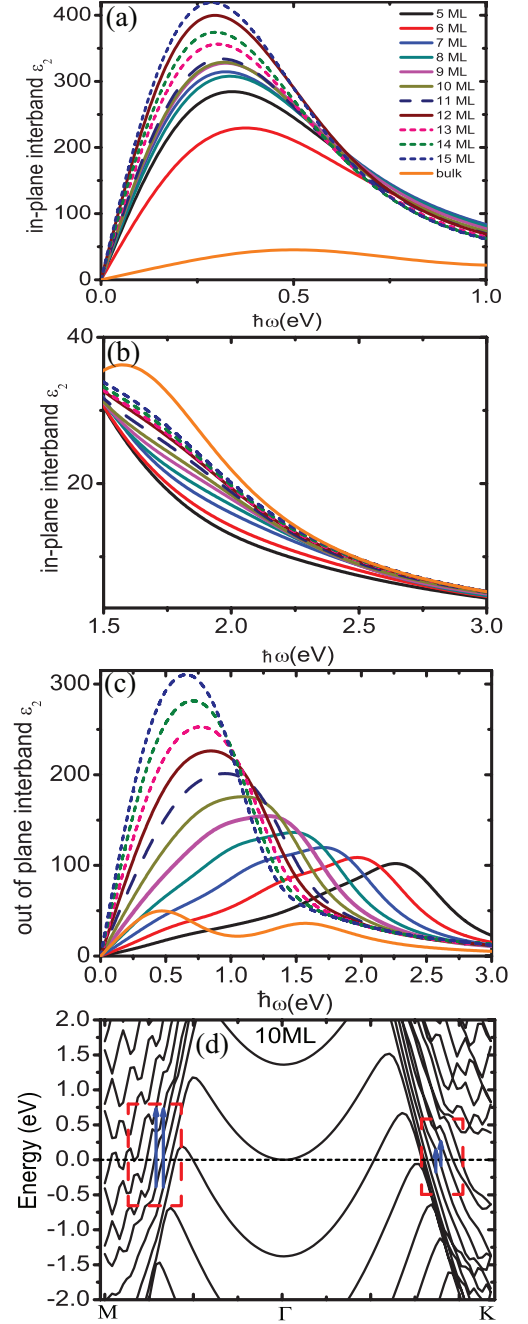


FIG. 4: Imaginary part of interband in-plane dielectric function of Al(111) films with the thickness from 5 ML to 15 ML (a) at low energy range and (b) relatively high energy range. (c) The imaginary part of interband out-of-plane dielectric function. For comparison, the bulk curve of dielectric function is also plotted in (a)-(c). (d) The band structure of 10 ML Al(111) film in order to track the optical transitions responsible for the peaks in its dielectric functions. The short arrows indicate the possible transitions between two parallel bands of ~ 0.3 eV energy difference and the long arrows indicate the possible transitions between two parallel bands of ~ 1.0 eV energy difference.

the bulk³². However, at $\hbar\omega = 1.5$ eV and $\hbar\omega = 3.0$ eV the value at large thickness is almost the same as the bulk value. This is due to the additional interband transitions in the film from the quantum-well states but absent in the bulk. It is inversely proportional to ω^2 from equation (1), giving rise to larger value in the low energy regime (this trend will be more clear from the dielectric function plot in Fig. 4 below). It's interesting to also note that at $\hbar\omega = 1.5$ eV and $\hbar\omega = 3.0$ eV the dielectric function is smaller for film thickness less than 15 MLs than that of bulk (see Fig. 3(b-c)). This lower dielectric constant will proportionally result in lower absorption loss. It suggests to us that ultrathin film can be used to achieve lower loss plasmonic devices in visible and UV frequency. In the film with thickness less than 4 MLs, the dielectric constant is significantly lower than the bulk value, indicating much stronger QSE modulation due to the strong quantum confinement perpendicular to the surface, where absorption loss will be the least. However, for such ultrathin film, the slab plasma frequency is larger as shown in Fig. 2(a) which will leads to larger damping induced energy loss. In Fig. 3(d-e) the out-of-plane interband ε_2 are showed. It is also much larger than the bulk at low photon energy ($\hbar\omega = 0.5$ eV) but very close to the bulk at higher energies ($\hbar\omega = 1.5$ eV and $\hbar\omega = 3.0$ eV). Therefore the symmetry breaking in ultrathin film will have significant influence on both the in-plane and out-of-plane ε_2 .

Finally in Fig. 4 we plotted the ε_2 for film thickness from 5 MLs to 15 MLs together with bulk interband ε_2 for comparison. Fig. 4(a) and Fig. 4(b) show the low energy part (≤ 1.0 eV) and high energy part (≥ 1.0 eV) of the in-plane interband ε_2 , respectively. In low energy range it is up to 10 times larger than the bulk value. This is consistent with the decreased slab plasma frequency in Fig. 2(a) which will result in larger interband ε_2 in some frequency range because of the f -sum rule in equation (5). Also the film in-plane dielectric function has a red-shifted peak position from 0.5 eV in bulk Al. For example, the peak is moved to ~ 0.28 eV for thickness of 15 MLs. Similarly in Fig. 4(c) the out-of-plane interband dielectric function ε_2 exhibits redshifted and enhanced peak compared to the peak of the bulk at 1.5 eV. The origin of this redshifted and enhanced peak is related to the band structure of the film. We have plotted the band structure of 10 ML film as a representative thickness in Fig. 4(d). Around Fermi energy parallel bands with en-

ergy difference of 0.3 eV and 1.0 eV are found, which are indicated by short and long arrows, respectively. The peak around 0.3 eV in the in-plane dielectric function plot for 10 ML film in Fig. 4(a) will be from the transitions in parallel bands with energy difference of 0.3 eV. The peak around 1.0 eV in the out-of-plane dielectric function plot for 10 ML film in Fig. 4(c) will be from the transitions in parallel bands with energy difference of 1.0 eV. The higher in-plane interband dielectric function ε_2 than the bulk counterpart indicates the larger absorption loss in the low energy range. On the other hand, from Fig. 4(b) we found in between 1.5 eV and 2.5 eV film interband ε_2 instead becomes larger than the bulk ε_2 . Therefore within this regime, lower absorption loss in plasmonics device is expected. For photon energy greater than 2.5 eV, the difference between films of different thickness and bulk is insignificantly small.

IV. CONCLUSION

We performed DFT calculations of the dielectric function of Al(111) ultrathin films of thickness from 1 to 39 MLs with RPA. Both the intraband and interband contributions to the total dielectric function were shown to be modulated by QSE through the calculation of slab plasma frequency and the imaginary part of the dielectric function, which are proportional to incident photon energy loss with free carrier damping mechanism and electron optical transition induced energy absorption mechanism, respectively. The key findings are: (1) in the low photon energy (≤ 1 eV) range, the interband transition energy loss is significantly enhanced compared to bulk value; however, (2) in a narrow relatively high energy range (1.5 eV to 2.5 eV) the in-plane interband transition energy is reduced and overall the thinner film is, the less the interband absorption of in-plane polarized light is for films less than 15 MLs. Our result may shed light on the search for low absorption loss plasmonics material through electronically tuning the band structure of metallic film by using different thickness.

This work was supported by NSF MRSEC (Grant No. DMR-1121252) and DOE-BES (Grant No. DE-FG02-04ER46148). We thank the CHPC at University of Utah and NERSC for providing the computing resources.

* Corresponding author. E-mail: fliu@eng.utah.edu

¹ F. K. Schulte, Surf. Sci., **55**, 427 (1976).

² Feng Liu, S. N. Khanna and P. Jena, Phys. Rev. B **42**, 976 (1990).

³ D. -A. Luh, T. Miller, J. J. Paggel, M. Y. Chou, T. -C. Chiang, Science **292**, 1131 (2001).

⁴ Hawoong Hong, C. -M. Wei, M. Y. Chou, Z. Wu, L. Basile, H. Chen, M. Holt and T. -C. Chiang, Phys. Rev. Lett., **90**,

076104 (2003).

⁵ H. Hu, H. Gao, and F. Liu, Phys. Rev. Lett. **109**, 106103 (2012).

⁶ Miao Liu, Yong Han, Lin Tang, Jin-Feng Jia, Qi-Kun Xue and Feng Liu, Phys. Rev. B **86**, 125427 (2012).

⁷ T. -L. Chan, C. Z. Wang, M. Hupalo, M. C. Tringides and K. M. Ho, Phys. Rev. Lett., **96**, 226102 (2006).

⁸ L.-Y. Ma, L. Tang, Ze-Lei Guan, Ke He, Kang An, Xu-Cun

- Ma, Jin-Feng Jia and Qi-Kun Xue, Y. Han, Steve Huang, and Feng Liu, Phys. Rev. Lett., **97**, 266102 (2006).
- ⁹ Xucun Ma *et al.*, PNAS 104, 9204 (2007).
- ¹⁰ Jungdae Kim, Shengyong Qin, Wang Yao, Qian Niu, M. Y. Chou and Chih-Kang Shih, PNAS **107**, 12761 (2010).
- ¹¹ M. Liu and F. Liu, Nanotechnology **25**, 135706 (2014).
- ¹² Paul R. West *et al.*, Laser Photonics Rev. **4**, 795 (2010).
- ¹³ Mark I. Stockman, Opt. Express **5**, 83 (2011).
- ¹⁴ Lukas Novotny and Niek van Hulst, Nature Photon. **19**, 22029 (2011).
- ¹⁵ J. Dryzek and A. Czapla, Phys. Rev. Lett. **58**, 721 (1987).
- ¹⁶ P. Apell and P. Ahlqvist, Physica Scripta **22**, 659 (1981).
- ¹⁷ Slimane Laref *et al.*, Opt. Express **21**, 11827 (2013).
- ¹⁸ L. A. Kuzik, V. A. Yakovlev, F. A. Pudonin and G. Mattei, Surf. Sci., **361**, 882 (1996).
- ¹⁹ L. A. Kuzik, V. A. Yakovlev, F. A. Pudonin and V. A. Yakovlev, JETP **78**, 114 (1994).
- ²⁰ D. A. Bobb *et al.*, Appl. Phys. Lett. **95**, 151102 (2009).
- ²¹ J. Harl, G. Kresse, L. D. Sun, M. Hohage and P. Zeppenfeld, Phys. Rev. B **76**, 035436 (2007).
- ²² G. Kresse and D. Joubert, Phys. Rev. B **59**, 1758 (1999).
- ²³ J. P. Perdew, J. A. Chevary, S. H. Vosko, K. A. Jackson, M. R. Pederson, D. J. Singh and C. Fiolhais, Phys. Rev. B **46**, 6671 (1992).
- ²⁴ G. Kresse and J. Furthmuller, Phys. Rev. B **54**, 11169 (1996).
- ²⁵ Cheol-Hwan Park, Catalin D. Spataru and Steven G. Louie, Phys. Rev. Lett. **96**, 126105 (2006).
- ²⁶ Li Yang, Nano Lett. **11**, 3844 (2011).
- ²⁷ Mauro Bruno, Maurizia Palummo, Andrea Marini, Rodolfo Del Sole, Valerio Olevano, Alexandre N. Kholod, and Stefano Ossicini, Phys. Rev. B **72**, 153310 (2005).
- ²⁸ Chaudia Ambrosch-Draxl and Jorge O. Sofo, Comput. Phys. Commun. **75**, 1 (2006).
- ²⁹ Li Yang, Jack Deslippe, Cheol-Hwan Park, Marvin L. Cohen and Steven G. Louie, Phys. Rev. Lett. **103**, 186802 (2009).
- ³⁰ Li Yang, Phys. Rev. B **81**, 155445 (2010).
- ³¹ J. Harl, "The linear response function in density functional theory: Optical spectra and improved description of the electron correlation", PhD dissertation at Universitat Wien, chapter 2 (2008).
- ³² Keun-Ho Lee and K. J. Chang, Phys. Rev. B **49**, 2362 (1994) and references therein.
- ³³ David Flötotto, Zumin Wang, Lars P. H. Jeurgens and Eric J. Mittemeijer, Phys. Rev. Lett. **109**, 045501 (2012).
- ³⁴ Yong Han and Da-Jiang Liu, Phys. Rev. B, **80**, 155404 (2009).
- ³⁵ Arisato Kawabata and Ryogo Kubo, J. Phys. Soc. Jpn. **21**, 1765 (1966).
- ³⁶ Michele Cini and P. Ascarelli, J. Phys. F **4**, 1998 (1974).
- ³⁷ D. M. Wood and N. W. Ashcroft, Phys. Rev. B **25**, 6255 (1982).
- ³⁸ Wen Chu Huang and Juh Tzeng Lue, Phys. Rev. B **49**, 17279 (1994).
- ³⁹ David Brust, Phys. Rev. B **2**, 818 (1970).
- ⁴⁰ Frank Szmulowicz and Benjamin Segall, Phys. Rev. B **24**, 892 (1981).